Heliyon 9 (2023) e21121

Contents lists available at ScienceDirect

Heliyon

journal homepage: www.cell.com/heliyon

Coupling coefficient calculation and optimization of positive rectangular series coils in wireless power transfer systems

Yang Leng [a,b], Derong Luo [a,**], Zhongqi Li [a], Fei Yu [c,*]

[a] College of Electrical and Information Engineering, Hunan University, Changsha, 410006, China
[b] College of Information Science and Engineering Changsha Normal University, Changsha, 410100, China
[c] School of Computer and Communication Engineering, Changsha University of Science and Technology, Changsha, 410114, China

ARTICLE INFO

Keywords:
Wireless power transfer (WPT)
Coupling coefficient
Coil misalignment
Positive series

ABSTRACT

In wireless power transfer (WPT) systems using magnetic coupling resonance, when there is a registration deviation between the transmitting and receiving coils, there will be significant fluctuations in the coupling coefficient, output power, and transmission efficiency, which will seriously affect the stability of the WPT system. The coupling coefficient is related to the length and width of the rectangular coil, number of turns, mutual geometric position, and space magnetic medium, making it difficult to maintain a constant value when the coil is offset. A single-emitter two-receiver positive-series rectangular coils structure and a method of calculating the structure are proposed. Then an optimization method for mutual inductance was proposed, and the structural parameters that met the design requirements were obtained using the proposed optimization method. The calculation formula for coupling coefficient was verified through simulation and experiments. The results showed that when the offset distance of the receiving coil along the *Y*-axis (driving direction) and *X*-axis reaches half of the length of the transmitting coil and 10 *cm*, the coupling coefficient, transmission efficiency, and output power remain almost unchanged.

1. Introduction

The wireless power transfer (WPT) technology provides an effective and feasible way to solve the safety problems caused by traditional contact charging, and provides applicable solutions to various vehicle models. The working frequency ranges from tens of kHz to MHz, and the transmission power can reach the megawatt level. The transmission distance is from centimeters to meters, and the transmission efficiency can be more than 96 % [1–3]. The position of the electrical equipment on the receiving side of such systems is not easy to be fixed, which usually has the problem with alignment, will cause the transverse and longitudinal offset or the transmission distance, and the coupling coefficient, output power and transmission efficiency will fluctuate greatly, the stability of the energy transmission system was affected seriously.

Coupled mode theory and mutual inductance theory are widely used to analyze various transmission performance of the WPT system. In Ref. [3], the authors proposed to increase the working range and change the trend about offset of flux by changing the structure of the asymmetric coil. A group in the University of Auckland in New Zealand proposed DD (double-D, DD) coils and DDQ

* Corresponding author.
** Corresponding author.
E-mail addresses: hdldr@sina.com (D. Luo), yufeiyfyf@csust.edu.cn (F. Yu).

https://doi.org/10.1016/j.heliyon.2023.e21121
Received 24 January 2023; Received in revised form 14 October 2023; Accepted 16 October 2023
Available online 17 October 2023

(double-D quadrature, DDQ) coils, which improves the coupling coefficient of the system [4]. BP (bipolar, BP) coils that have similar results and the cost is low [5], and improved TP (tripolar, TP) coils [6]. The coil shown in Ref. [7] is proposed by Ahmad and others. Because of its symmetrical structure, it has better anti-drift ability in both directions. The structure which triangular coils are placed symmetrically along the diagonal line to improve the diagonal migration ability is proposed in Ref. [8]. Multiple small-size coils are arranged to form a coil array, only the coil close to the receiving coil transmits energy. In this way, the relative offset between single coils on the primary secondary side is reduced [9,10]. In Ref. [11], a magnetic flux tube coupling structure is constructed by using a strip magnetic core. Its coupling coefficient is larger than that of a circular coil, and it has stronger anti-migration ability on the horizontal plane. In Ref. [12], the structure of winding five coils in series on the H-shaped magnetic core is proposed to improve the anti-drift ability of the flat solenoid coil in the Y direction. In Ref. [13], the coupling structure with magnetic core is used to maintain mutual inductance continuously, the offset range is 40 % of the maximum value, and the mutual inductance fluctuation is only 5 %. Chen et al. proposed an algorithm based on reverse series coil in finite element simulation [14]. In order to increase the effective charging area of a single coil and improve the smoothness of mutual induction when the position migrated, the turn-by-turn optimization and turn-by-coil group method is proposed in Ref. [15]. A dynamic and static wireless power transfer system superimposed dislocation coil (SDC) structure is proposed in Ref. [16], it ensures a constant coupling coefficient.

In this paper, a single-emitter two-receiver positive-series rectangular coils structure and a method of calculating the structure are proposed. Then an optimization method of the mutual inductance is presented, the parameters of the proposed structure that meet the design requirements are obtained by using the proposed optimization method. The coupling coefficient calculation formula is verified by simulation and experiment, these results show that the coupling coefficient, transmission efficiency and output power remain almost constant when the misalignment distance of the receiving coil along the *Y*-axis (driving direction) and *X*-axis reaches half of the length of the transmitting coil and 10 *cm*.

1.1. The structure of rectangular coils

In order to keep the coupling coefficient constant when the misalignment distance of the receiving coil along the *Y*-axis (driving direction) and *X*-axis reaches half of the length of the transmitting coil and 10 *cm*, a new coil structure is proposed in this section.

The new structure is shown in Fig. 1. The transmitting coil is T_x, and the receiving coils are made of R_{x1} and R_{x2} in positive series, and the size of R_{x1} and R_{x2} is the same. O and O_1 are the center of the transmitting and receiving coils, I_1 and I_2 are the currents of R_{x1} and R_{x2} that in the same direction.

Fig. 2 shows the coils of the new structure. T_x is the transmitting coil, R_{x1} and R_{x2} are the receiving coils. $l_{1\text{-inner}}$ and $l_{2\text{-inner}}$ are the inner length of R_{x1} and R_{x2}, and $l_{3\text{-inner}}$ is the inner length of T_x. $h_{1\text{-inner}}$ and $h_{2\text{-inner}}$ are the inner width of R_{x1} and R_{x2}, and $h_{3\text{-inner}}$ is the inner width of T_x. $l_{1\text{-outer}}$ and $l_{2\text{-outer}}$ are the outer length of R_{x1} and R_{x2}, and $l_{3\text{-outer}}$ is the outer length of T_x. $h_{1\text{-outer}}$ and $h_{2\text{-outer}}$ are the outer width of R_{x1} and R_{x2}, and $h_{3\text{-outer}}$ is the outer width of T_x.

According to the definition of self-inductance and mutual-inductance, the total self-inductance of R_x can be calculated as follows:

$$L_{Rx} = L_{Rx1} + L_{Rx2} + 2M_{Rx1-Rx2} \tag{1}$$

The total mutual inductance between T_x and R_x can be calculated as follows:

$$M_{Tx-Rx} = M_{Tx-Rx1} + M_{Tx-Rx2} \tag{2}$$

where L_{Tx}, L_{Rx1} and L_{Rx2} are the self-inductance of T_x, R_{x1} and R_{x2} respectively. $M_{Tx\text{-}Rx1}$ is the mutual-inductance between T_x and R_{x1}, and $M_{Tx\text{-}Rx2}$ is the same between T_x and R_{x2}.

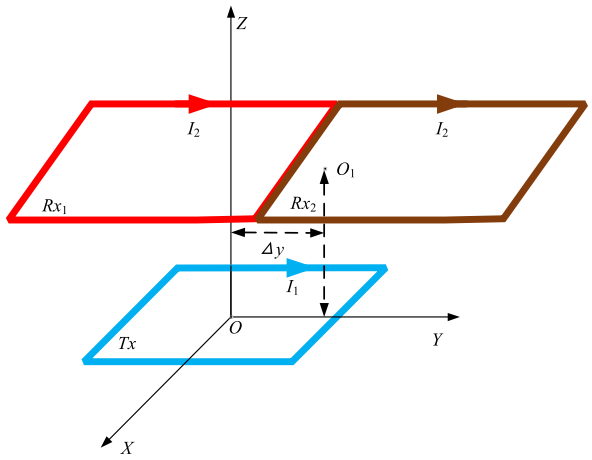

Fig. 1. Schematic diagram of single-emitter two-receiver positive-series rectangular coils.

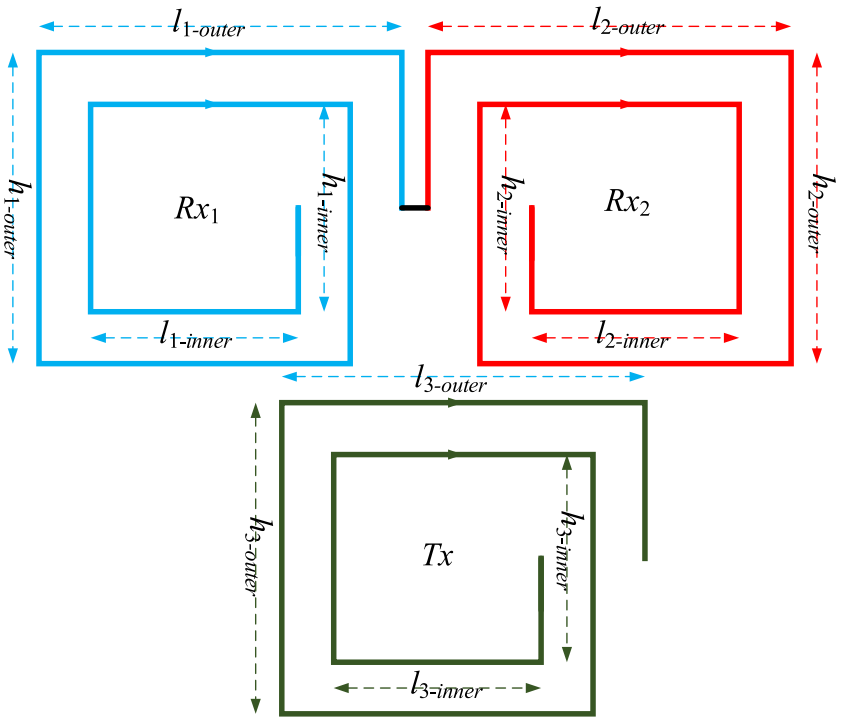

Fig. 2. Positive series rectangular coils structure.

$$k_{12} = \frac{M_{12}}{\sqrt{L_1 L_2}} \tag{3}$$

where k_{12} is the coupling coefficient between the two coils, M_{12} is the mutual-inductance, and L_1, L_2 are self-inductance.

The formula for the coupling coefficient of the new structure is:

$$k_{Tx-Rx} = \frac{M_{Tx-Rx}}{\sqrt{L_{Tx} L_{Rx}}} = \frac{M_{Tx-Rx1} + M_{Tx-Rx2}}{\sqrt{L_{Tx}(L_{Rx1} + L_{Rx2} + 2M_{Rx1-Rx2})}} = k_{Tx-Rx1} + k_{Tx-Rx2} \tag{4}$$

where $k_{Tx\text{-}Rx1}$ is the coupling coefficients between T_x and R_{x1} and $k_{Tx\text{-}Rx2}$ is the coupling coefficients between T_x and R_{x2}.

2. Calculation of coupling coefficients

In this section, a calculation method is proposed, which is used calculate the coupling coefficient of the new structure quickly.

(a) The self inductance of the rectangular coil

Fig. 3 shows the structure of a single rectangular coil, a_1 and a_2 are the half-length and half-width of $Coil_1$. $Coil_1$ consists of four parts

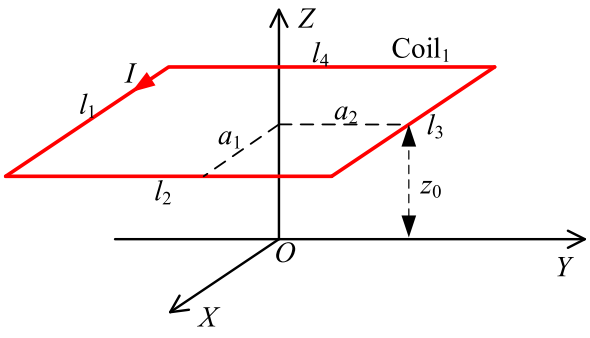

Fig. 3. Schematic diagram of a single rectangular coil.

(l_1, l_2, l_3, l_4). Z_0 is the height of the rectangular coil from the O point plane. I is the current of $Coil_1$.

The magnetic vector of any point P (x, y, z) is as follows:

$$A(x,y,z)=\frac{\mu_0}{4\pi}\int_v\frac{J(x',y',z')dv'}{R} \tag{5}$$

where J is the current density and v is the current distribution of the $Coil_1$. R is the distance from P (x, y, z) to the source point (x', y', z').

$$R=\sqrt{(x-x')^2+(y-y')^2+(z-z')^2} \tag{6}$$

The dual Fourier transformation and its inverse transformation are used to solve (5):

$$b(\xi,\eta,z)=\int_{-\infty}^{\infty}\int_{-\infty}^{\infty}B(x,y,z)\cdot e^{-\mathrm{j}(x\xi+y\eta)}dxdy \tag{7}$$

$$B(x,y,z)=\frac{1}{4\pi^2}\int_{-\infty}^{\infty}\int_{-\infty}^{\infty}b(\xi,\eta,z)\cdot e^{\mathrm{j}(x\xi+y\eta)}d\xi d\eta \tag{8}$$

Substituting (5) into (7):

$$a(\xi,\eta,z)=\frac{\mu_0}{2}\int_v\frac{1}{k}e^{-j(x'\xi+y'\eta)}J(x',y',z')e^{-k|z-z'|}dv' \tag{9}$$

where $k=\sqrt{\xi^2+\eta^2}$. The relationship between the incident magnetic flux density and the magnetic vector potential is as follows:

$$B=\nabla\times A \tag{10}$$

Substituting the Fourier transform into (10):

$$\begin{cases} b_x=-j\eta a_z-\dfrac{\partial a_y}{\partial z} \\ b_y=\dfrac{\partial a_x}{\partial z}+j\xi a_z \\ b_z=-j\xi a_y+j\eta a_x \end{cases} \tag{11}$$

The component a_x of the magnetic vector potential in the X-axis direction is generated only by the wires l_1 and l_3 which are parallel to the X-axis. The expression of a_x is as follows:

$$a_x=a_{x_1}-a_{x_3}=\frac{\mu_0 Ie^{ja_2\eta}e^{-|z-z_0|k}}{2k}\left(\int_{-a_1}^{a_1}e^{-jx'\xi}dx'-\int_{-a_1}^{a_1}e^{-jx'\xi}dx'\right)=\frac{j2\mu_0 I\sin(\xi a_1)\sin(\eta a_2)e^{-|z-z_0|k}}{\xi k} \tag{12}$$

where a_{x1} and a_{x3} represent the magnetic vector potential components, which are generated by wires l_1 and l_3 respectively.

Similarly, the component of the magnetic vector potential a_y in the Y-axis direction is:

$$a_y=\frac{-j2\mu_0 I\sin(\eta a_2)\sin(\xi a_1)e^{-|z-z_0|k}}{\eta k} \tag{13}$$

Substituting (12) and (13) into (11):

$$\begin{cases} b_x=\dfrac{j2\mu_0 I\sin(\xi a_1)\sin(\eta a_2)}{\eta} \\ b_y=\dfrac{j2\mu_0 I\sin(\xi a_2)\sin(\eta a_1)}{\xi} \\ b_z=\dfrac{-2\mu_0 Ik\sin(\xi a_1)\sin(\eta a_2)}{\xi\eta} \end{cases} \tag{14}$$

Substituting (14) into (8), the magnetic flux density in the $z=z_0$ plane is:

$$\begin{cases} B_x = \dfrac{1}{4\pi^2}\displaystyle\int_{-\infty}^{\infty}\int_{-\infty}^{\infty}\frac{j2\mu_0 I\,\sin(\xi a_1)\sin(\eta a_2)}{\eta}e^{j(x\xi+y\eta)}d\xi d\eta \\ B_y = \dfrac{1}{4\pi^2}\displaystyle\int_{-\infty}^{\infty}\int_{-\infty}^{\infty}\frac{j2\mu_0 I\,\sin(\xi a_2)\sin(\eta a_1)}{\xi}e^{j(x\xi+y\eta)}d\xi d\eta \\ B_z = \dfrac{1}{4\pi^2}\displaystyle\int_{-\infty}^{\infty}\int_{-\infty}^{\infty}\frac{-2\mu_0 Ik\,\sin(\xi a_1)\sin(\eta a_2)}{\xi\eta}e^{j(x\xi+y\eta)}d\xi d\eta \end{cases} \tag{15}$$

For a single rectangular coil, only the magnetic flux density in the Z-axis direction needs to be considered. According to (16), the self-inductance is obtained as follows:

$$\begin{aligned} L &= \frac{1}{I}\oiint B_z ds \\ &= \frac{1}{4\pi^2}\int_{-\infty}^{\infty}\int_{-\infty}^{\infty}\int_{-a_1}^{a_1}\int_{-a_2}^{a_2}\frac{-2\mu_0 Ik\,\sin(\xi a_1)\sin(\eta a_2)}{\xi\eta}e^{j(x\xi+y\eta)}dydxd\xi d\eta \end{aligned} \tag{16}$$

(b) Mutual inductance calculation method of the rectangular coil

Fig. 4 is the schematic diagram of the two rectangular coils, including $Coil_1$ and $Coil_2$. a_1 and a_2 are half-length and half-width of $Coil_1$. b_1 and b_2 are half-length and half-width of $Coil_2$. $Coil_1$ consists of four parts (l_1, l_2, l_3, l_4), the center is O_1. $Coil_2$ consists of four parts (L_1, L_2, L_3, L_4), and the center is O_2. S_1 is the vertical distance between O and O_1, and S_2 is the vertical distance between O and O_2.

The mutual inductance between $Coil_1$ and $Coil_2$ can be obtained.

$$M_{12} = \oiint_D B\cdot ds / I = \frac{1}{4\pi^2 I}\int_{-\infty}^{\infty}\int_{-\infty}^{\infty}(C_{iz}+C_{ix})\cdot\frac{e^{j(b_{1d}+b_1)\xi}-e^{j(b_{1d}-b_1)\xi}}{j\xi}\cdot\frac{e^{j(b_{2d}+b_2)\eta}-e^{j(b_{2d}-b_2)\eta}}{j\eta}\cdot e^{-ks_2}d\xi d\eta \tag{17}$$

where b_{1d} and b_{2d} are the misalignment of the X-axis and Y-axis respectively. The mutual inductance $M_{Tx\text{-}Rx1}$ between T_x and R_{x1}, and $M_{Tx\text{-}Rx2}$, $M_{Rx1\text{-}Rx2}$ can be calculated by (17).

The mutual inductance between multiturn coils can be calculated by (18).

$$M = \sum_{m=1}^{N_1}\sum_{n=1}^{N_2}M_{mn} \tag{18}$$

where N_1 is the number of turns of $Coil_1$, N_2 is the number of turns of $Coil_2$, m is the m-th turn of $Coil_1$, and n is the n-th turn of $Coil_2$.

Fig. 5 shows the circuit diagram of the coils, L_1 and R_1 are self-inductance resistance of transmitting coil respectively, L_3 and R_3 are self-inductance resistance of receiving coil, C_{Tx} and C_{Rx} are resonant capacitance of transmitting and receiving coil, M_{13} is mutual inductance of transmitting and receiving coil, R_S is internal resistance of source, V_S is voltage source, R_L is resistance of load.

The kirchhoff equation of electric voltage is

$$\begin{bmatrix} Z_1 & j\omega M_{13} \\ j\omega M_{13} & Z_3 \end{bmatrix}\begin{bmatrix} I_1 \\ I_3 \end{bmatrix} = \begin{bmatrix} V_S \\ 0 \end{bmatrix} \tag{19}$$

The current I_1 and I_2 of transmitting and receiving coil can be calculated by

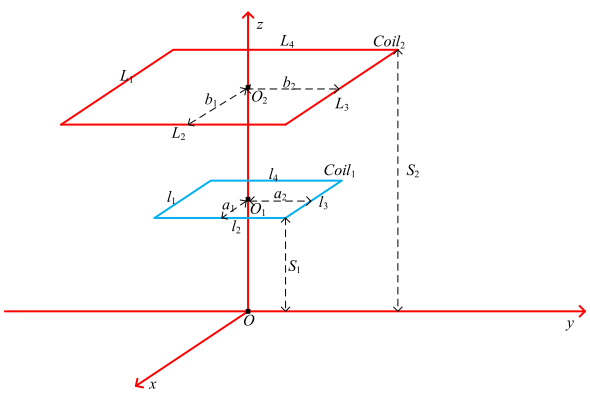

Fig. 4. Schematic diagram of two rectangular coils.

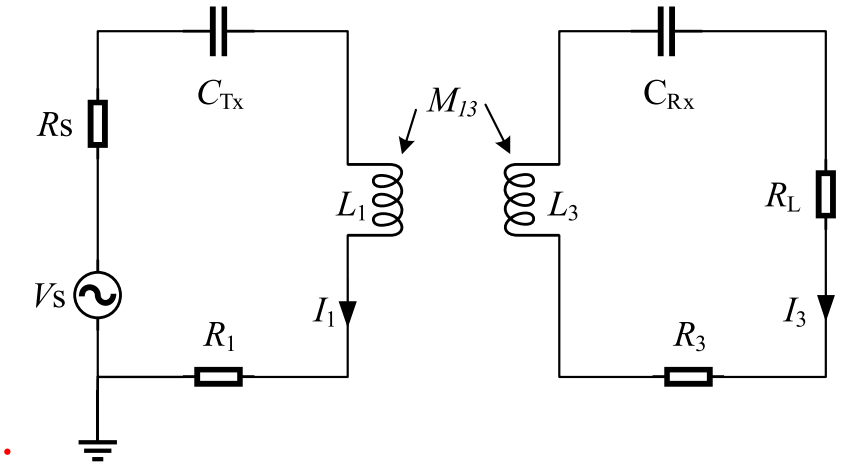

Fig. 5. Circuit diagram of coils.

$$\begin{cases} I_1 = \dfrac{Z_3 V_S}{Z_1 Z_3 + (\omega M_{13})^2} \\ I_3 = -\dfrac{j\omega M_{13} V_S}{Z_1 Z_3 + (\omega M_{13})^2} \end{cases} \tag{20}$$

where ω is the working frequency.

The output voltage can be calculated by (21):

$$V_L = \frac{-j\omega M V_S R_L}{(R_S + R_1)(R_2 + R_L) + (\omega M)^2} \tag{21}$$

The transmission efficiency can be calculated by (22):

$$\eta = \frac{{I_3}^2 R_L}{V_S I_1} = \frac{(\omega M_{13})^2 R_L}{{Z_1 Z_3}^2 + (\omega M_{13})^2 Z_3} \tag{22}$$

Fig. 6 shows the electrical circuit and the configuration of the WPT system. Fig. 7(a) shows that the normalized $k_{Tx\text{-}Rx}$ of the new structure, the increase of the $k_{Tx\text{-}Rx1}$ is more than the decrease of the $k_{Tx\text{-}Rx2}$ when Δy is small, on the contrary When Δy is large. The Δy larger than it in Ref. [16] about the coupling $k_{Tx\text{-}Rx}$ is approach to 1. Fig. 7(b) shows the results of the traditional structure. The coupling $k_{Tx\text{-}Rx}$ decreases monotonically with the increase of Δy.

The simulation parameters that $l_{1\text{-}inner}$ is 18–22 *cm*, $h_{1\text{-}inner}$ is 48–52 *cm*, $l_{3\text{-}inner}$ and $h_{3\text{-}inner}$ is 16–20 *cm*, and the step is 1 *cm*. N_1 is 28–32, N_2 is 19–23, and the step is 1.

Fig. 8 shows that the $k_{Tx\text{-}Rx}$ and mutual inductance of the structure.

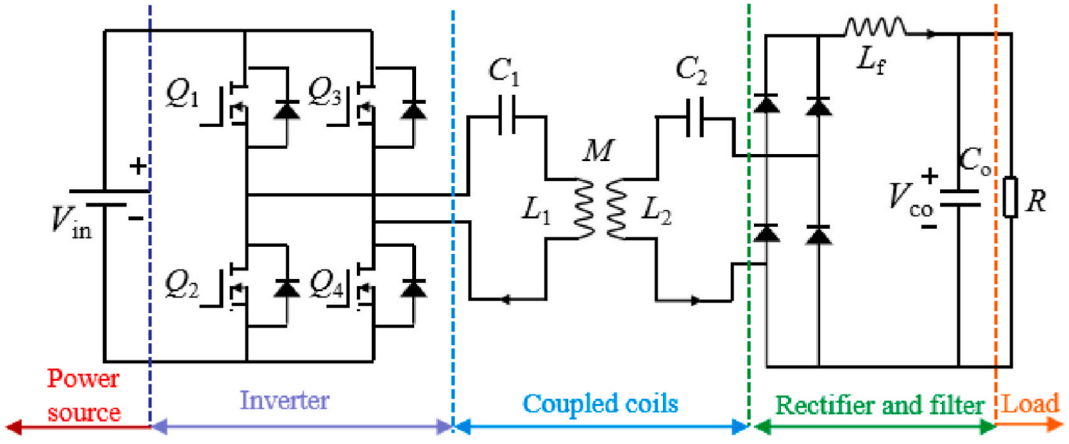

Fig. 6. The circuit and the configuration of the WPT system.

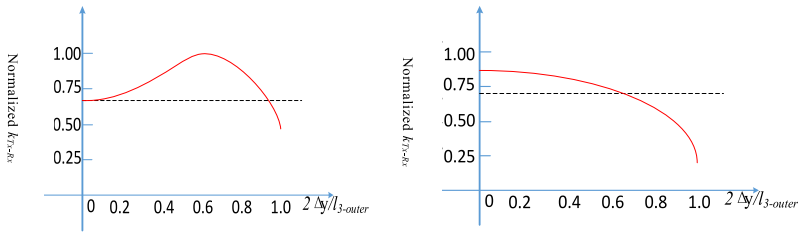

(a) the new structure (b) the traditional structure

Fig. 7. Diagram of normalization for coupling coefficient.

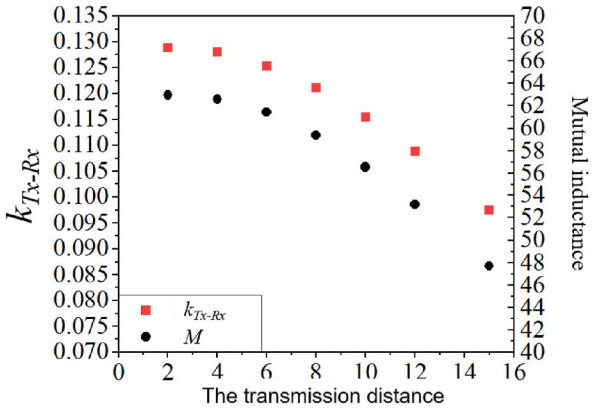

Fig. 8. Diagram of $k_{Tx\text{-}Rx}$ and mutual inductance.

3. Optimization method of the mutual inductance

The variation of the coupling coefficient of the misalignment distance of the receiving coil along the *Y*-axis (driving direction) and *X*-axis are analyzed.

(a) optimization methods and steps

(1) Initialization parameters and constraints: the transmission distance between T_x and R_x is 15 *cm*. The diameter of copper wire is 0.25 *cm*.

$$\varepsilon_{1\_Y} = (k_{Tx-Rx-max\_Y} - k_{Tx-Rx-0}) / k_{Tx-Rx-0} \tag{23}$$

$$\varepsilon_{2\_Y} = (k_{Tx-Rx-min\_Y} - k_{Tx-Rx-0}) / k_{Tx-Rx-0} \tag{24}$$

$$\varepsilon_{1\_X} = (k_{Tx-Rx-max\_X} - k_{Tx-Rx-0}) / k_{Tx-Rx-0} \tag{25}$$

$$\varepsilon_{2\_X} = (k_{Tx-Rx-min\_X} - k_{Tx-Rx-0}) / k_{Tx-Rx-0} \tag{26}$$

where the coupling coefficient fluctuation rate of misalignment distance of the receiving coil along the *X*-axis, *Y*-axis are $\varepsilon 1\_X$, $\varepsilon 2\_X$, $\varepsilon 1\_Y$ *and* $\varepsilon 2\_Y$. $k_{Tx\text{-}Rx\text{-}0}$ is coupling coefficient when misalignment distance is 0(Δx=Δy=0), $k_{Tx\text{-}Rx\text{-}max\_Y}$ and $k_{Tx\text{-}Rx\text{-}min\_Y}$ are the maximum and minimum value of the coupling coefficients when the misalignment distance of the receiving coil along the *Y*-axis(Δy) is less than half of the length of the transmitting coil. $k_{Tx\text{-}Rx\text{-}max\_X}$ and $k_{Tx\text{-}Rx\text{-}min\_X}$ are the maximum and minimum value of the coupling coefficients when the misalignment distance of the receiving coil along the *X*-axis(Δx) is less than 10 *cm*.

(2) Calculation: The coupling coefficient is calculated by (4), the coupling coefficient fluctuation rates are calculated by (23)-(26).

(3) Loop execution: The program uses a loop execution to find out the maximum of the parameters is determined by the constraints. The constraints are $\varepsilon 1\_Y<\varepsilon 1\_Y^*$, $\varepsilon 2\_Y<\varepsilon 2\_Y^*$, $\varepsilon 1\_X<\varepsilon 1\_X^*$, $\varepsilon 2\_X<\varepsilon 2\_X^*$ and $kTx\text{-}Rx\text{-}0 > kTx\text{-}Rx\text{-}0^*$. The maximum fluctuation rate that $\varepsilon 1\_X^*$, $\varepsilon 2\_X^*$, $\varepsilon 1\_Y^*$, $\varepsilon 2\_Y^*$ *are* set to 5 %.

(4) Save results and parameters: The simulation results and the output are saved.

The optimization method of the coupling coefficient is shown in Fig. 9.

(b) Optimized result

Fig. 10(a) shows the fluctuation rate results when R_x is migrated along the X-axis, when the step size is 30, the coupling coefficient is high, and when $\Delta x = 10\ cm$, the coupling coefficient fluctuation reaches the maximum 4.78 %. Fig. 10(b) shows the results when R_x is migrated along the Y-axis, the fluctuation reaches the maximum and is only 4.5 %. Fig. 10(c) shows the coupling coefficient when R_x is migrated along the X-axis, Fig. 10(d) shows the coupling coefficient when R_x is migrated along the Y-axis, when $\Delta x = \Delta y = 0$, $k_{Tx\text{-}Rx}$ is 0.099.

4. Verification

The simulation was carried out using Ansys Maxwell 15.0, and the model was shown in Fig. 11. The parameters of coils are listed in Table 1. The simulation results of R_x is migrated along the X-axis and Y-ax are listed in Table 2 and Table 3 respectively.

The experimental device is shown in Fig. 12, and the diagram of Tx coil is shown in Fig. 13(a), Rx *is* shown in Fig. 13(b). The transmission distance between T_x and R_x is set to 15 *cm*. The resistance (R_L) is set to 40Ω and the voltage is set to 45V.

The Tx input voltage (U_1), current (I_1), Rx output voltage (U_2), current (I_2) were measured by WT5000 power analyzer of Yokogawa Electric machinery. The parameters of resonant coil measured by impedance analyzer are listed in Table 4. The traditional structure consists of T_x and R_x, and the coil parameters are shown in Table 5.

Fig. 14(a) shows the calculated, simulated and measured coupling coefficient of the new structure when R_x is migrated along the X-axis. Fig. 14(b) shows the results when R_x is migrated along the Y-axis. The coupling coefficient is decrease When Δx is increase, but is increase and then decrease When Δy is increase. The maximum fluctuation of the coupling coefficient of R_x migration along the X-axis is 4.52 % and it is 4.92 % along the Y-axis.

Fig. 15(a) shows the calculated, simulated and measured coupling coefficient of the traditional structure when R_x is migrated along the X-axis. Fig. 15(b) shows the results when R_x is migrated along the Y-axis. The results are basically consistent and stable at about 0.12. The maximum fluctuation of the coupling coefficient of R_x migration along the X-axis is 4.52 %. However, the maximum fluctuation of the coupling coefficient along the Y-axis is 15 %, which is much larger than 5 %.

Fig. 16(a) shows the transmission efficiency (η) of the new structure and traditional structure when R_x is migrated along the X-axis, Fig. 16(c) shows the results when R_x is migrated along the Y-axis. The transmission efficiency (η) of the new structure is basically the same as that of the traditional structure.

Fig. 16(b) shows the output power (P_{out}) of the new structure and traditional structure when R_x is migrated along the X-axis, Fig. 16 (d) shows the results when R_x is migrated along the Y-axis. The fluctuation of the new structure migration along the Y-axis is far less than that of the traditional structure.

The performance comparison between the proposed structure and the structures proposed in other references is shown in Table 6. Compared with Ref. [16], the single-emitter two-receiver positive-series rectangular coils structure has low cost, and the fluctuation rate of coupling coefficient, transmission efficiency and output power are similar. Compared with Refs. [17–19], the single-emitter two-receiver positive-series rectangular coils structure has the smallest fluctuation rate of coupling coefficient, transmission efficiency and output power.

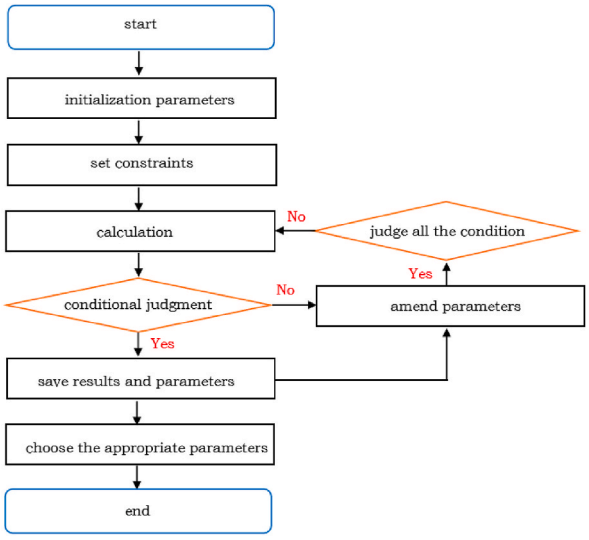

Fig. 9. Diagram of process for optimization of coupling coefficient.

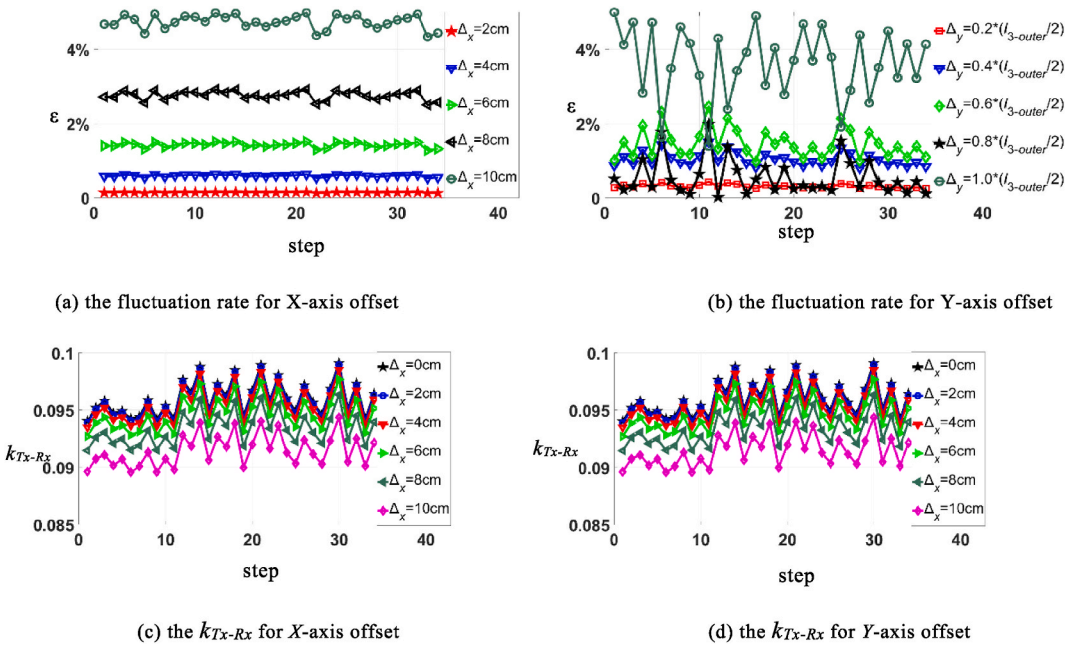

(a) the fluctuation rate for X-axis offset

(b) the fluctuation rate for Y-axis offset

(c) the $k_{Tx\text{-}Rx}$ for X-axis offset

(d) the $k_{Tx\text{-}Rx}$ for Y-axis offset

Fig. 10. Diagram of optimization of simulation.

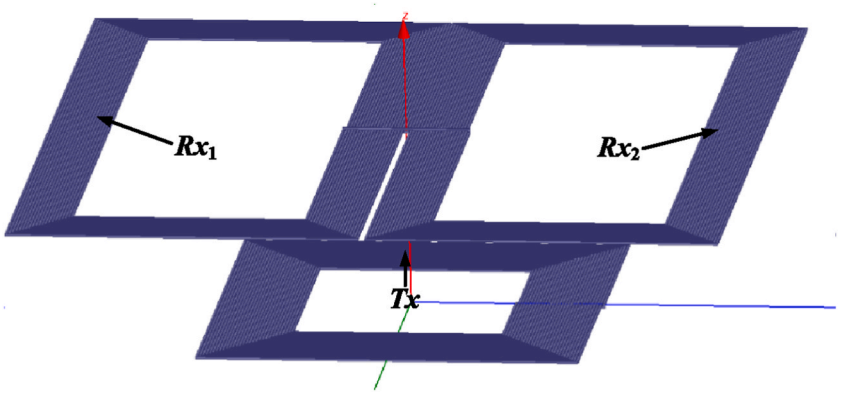

Fig. 11. Simulation model.

Table 1
Parameters of coils.

Coil	inner lengths(*cm*)	inner width(*cm*)	outer length(*cm*)	outer width(*cm*)	turn	diameter(*cm*)
T_x	18	18	32.5	32.5	30	0.25
R_{x1}	20	50	30	60	21	0.25
R_{x2}	20	50	30	60	21	0.25

5. Conclusions

In this paper, the new structure of a single-emitter two-receiver positive-series rectangular coils and a method of calculating the structure are proposed. The coupling coefficient characteristics are analyzed, the coil parameters of the structure are optimized, the experimental results verify the feasibility and superiority of the coupling coefficient calculation and coupling coefficient optimization method.

The coupling coefficient of the new structure is basically constant, the maximum coupling coefficient fluctuation rate is the same as the traditional structure migration along the X-axis, it is much less than the traditional structure along the Y-axis. The transmission efficiency of traditional structure and new structure is basically constant, the output power of the new structure is much larger than

Table 2
Simulation for X misalignment.

$\Delta x(cm)$	L_{Tx} (uH)	L_{Rx} (uH)	$M_{Tx\text{-}Rx}(uH)$	$k_{Tx\text{-}Rx}$	ε
−10	362.63	654.02	45.071	0.09255	4.11 %
−8	362.51	653.77	45.974	0.09444	2.19 %
−6	362.47	653.94	46.548	0.09610	0.97 %
−4	362.56	653.96	46.881	0.09628	0.26 %
−2	362.6	654.04	46.918	0.09634	0.18 %
0	362.64	654	47.003	0.09652	0
2	362.6	654.04	47.018	0.09634	0.18 %
4	362.56	653.96	46.881	0.09628	0.26 %
6	362.47	653.94	46.548	0.09610	0.97 %
8	362.51	653.77	45.974	0.09444	2.19 %

Table 3
Simulation for Y misalignment.

$\Delta y(cm)$	L_{Tx} (uH)	L_{Rx} (uH)	$M_{Tx\text{-}Rx}(uH)$	$k_{Tx\text{-}Rx}$	ε
0	362.64	654	47.003	0.09652	0
1.625	362.33	654.18	47.085	0.09671	0.17 %
3.25	362.69	654	47.188	0.09689	0.39 %
4.875	362.33	654.21	47.437	0.09743	0.92 %
6.5	362.58	654.01	47.675	0.0979	1.43 %
8.125	363.1	655.7	47.937	0.09824	1.99 %
9.75	362.93	656.86	48.631	0.0996	3.46 %
11.375	362.38	656.74	47.989	0.09837	2.10 %
13	362.49	654.01	47.749	0.09807	1.59 %
14.675	362.78	654.85	47.198	0.09683	0.41 %
16.25	362.96	654.9	46.144	0.09465	1.83 %

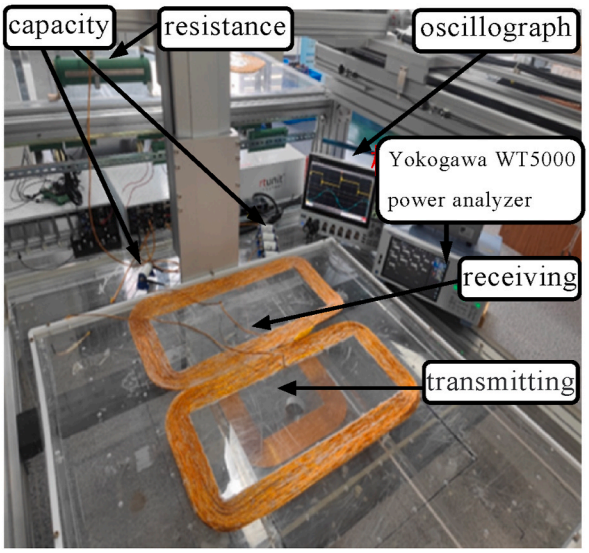

Fig. 12. Experimental device.

that of the traditional structure, and the fluctuation rate of is much smaller than the traditional structure. In conclusion, the new structure has a higher output power and an anti-*Y* offset.

The maximum misalignment distance of the new structure of the receiving coil along the *Y*-axis is half of the length of the transmitting coil, and the transmission efficiency and output power of the new structure can be kept almost constant, and the output power of the new structure is far greater than the traditional structure. This will save the cost of wireless power transfer systems greatly and reduce the difficulty of controlling. Therefore, the new structure can satisfy the dynamic and static radio charging requirements of electric cars. In the future research, we should improve the structure to receive a larger coupling coefficient and keep the coupling coefficient constant of greater distance.

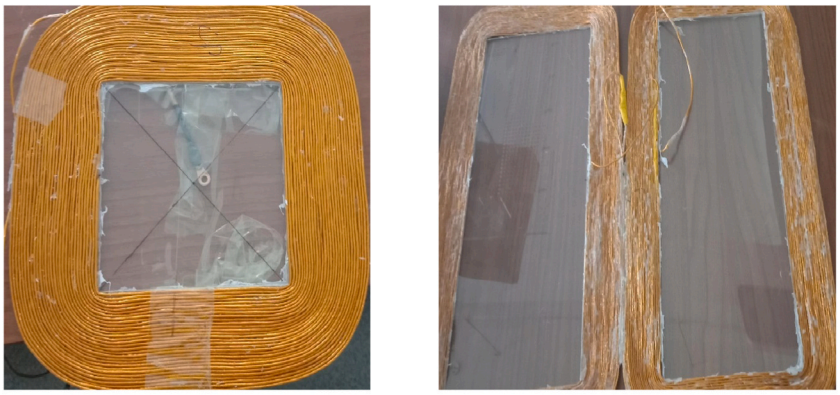

(a) *Tx* (b) *Rx*

Fig. 13. Diagram of coils.

Table 4
Measurement for experimental.

Parameters	Significance	Value
$L_1/\mu H$	self inductance of *Tx*	360.30
$L_2/\mu H$	self inductance of *Rx* in new structure	650.01
$L_3/\mu H$	self inductance of *Rx* in traditional structure	597.72
C_1/nF	compensating capacity of *Tx*	9.665
C_2/nF	compensating capacity of *Rx* about new structure	5.360
C_3/nF	compensating capacity of *Rx* about traditional structure	5.860
$R_1/m\Omega$	parasitic resistance of *Tx*	264.44
$R_2/m\Omega$	parasitic resistance of *Rx* about new structure	382.20
$R_3/m\Omega$	parasitic resistance of *Rx* about traditional structure	510.90
f_0/kHz	resonance frequency	85.0

Table 5
Parameters of coil.

Coil	inner lengths(*cm*)	inner width(*cm*)	outer length(*cm*)	outer length(*cm*)	turn	diameter(*cm*)
T_x	18	18	32.5	32.5	30	0.25
R_x	50	50	60	60	21	0.25

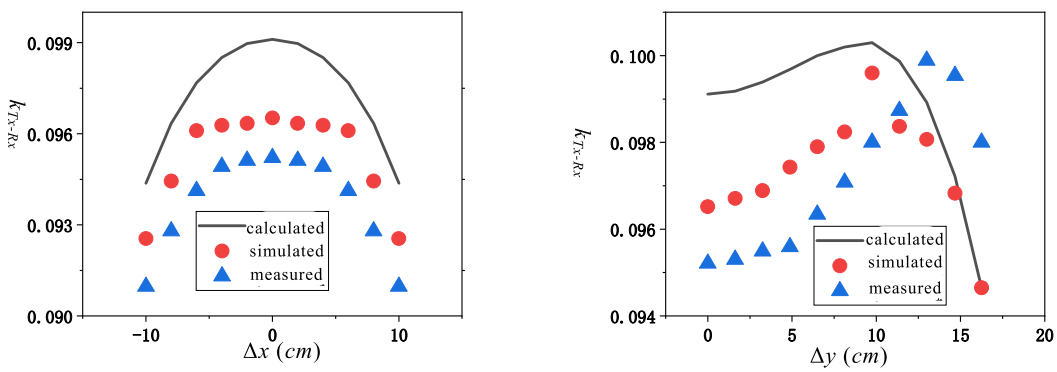

(a) $k_{Tx\text{-}Rx}$ *of Rx migrated along the X-axis* (b) $k_{Tx\text{-}Rx}$ *of Rx is migrated along the Y-axis*

Fig. 14. Diagram of coupling coefficient for new structure.

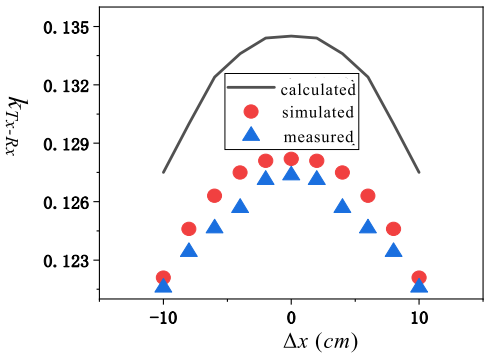

(a) $k_{Tx\text{-}Rx}$ *of Rx migrated along the X-axis*

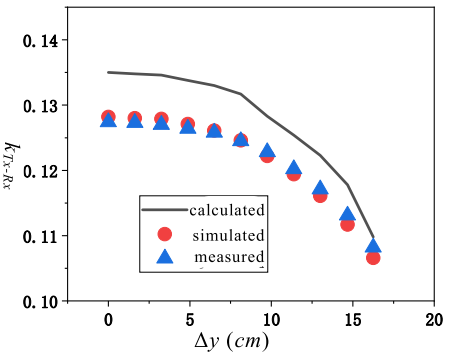

(b) $k_{Tx\text{-}Rx}$ *of Rx is migrated along the Y-axis*

Fig. 15. Diagram of coupling coefficient for traditional structure.

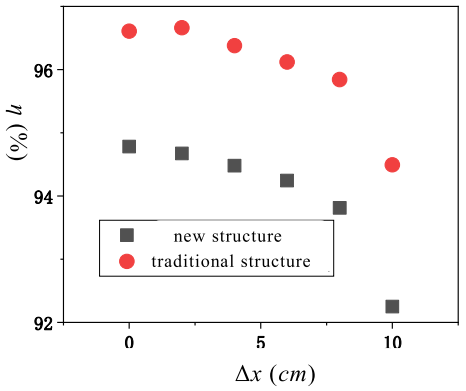

(a)*η of Rx migrated along the X-axis*

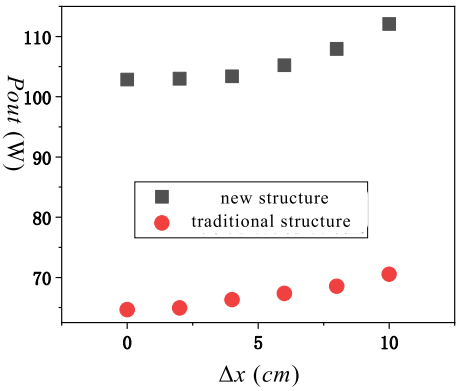

(b) *Pout of Rx is migrated along the X-axis*

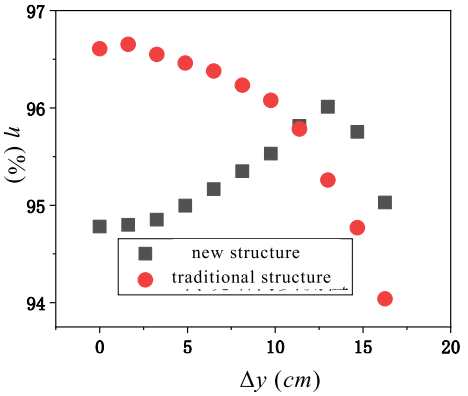

(c) *η of Rx migrated along the Y-axis*

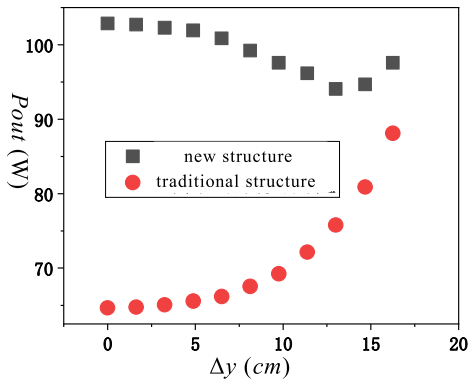

(d) *Pout of Rx is migrated along the Y-axis*

Fig. 16. Diagram of results for experimental.

Table 6
Performance comparison.

References	Size of *Tx* (Length*Width)	Size of *Rx* (Length*Width)	Maximum misalignment	Fluctuation of Coupling coefficient	Fluctuation of output power	Fluctuation of efficiency
[16]	35 *cm*358 *cm*	66 *cm*62 *cm*	17.5 *cm*	3.12 %	7.93 %	2.79 %
[17]	30 *cm*20 *cm*	100 *cm*80 *cm*	24 *cm*	/	50.0 %	30.0 %
[18]	Diameter:38 *cm*	Diameter:60 *cm*	24 *cm*	8.4 %	14.2 %	2.8 %
[19]	30 *cm*30 *cm*	60 cm*60 *cm*	20 *cm*	15.0 %	/	/
Our work	32.5 *cm*32.5 *cm*	60 cm*60 *cm*	16.25 *cm*	4.52 %	9.48 %	3.78 %

Data availability statement

Data will be made available on request.

CRediT authorship contribution statement

Yang Leng: Conceptualization, Data curation, Formal analysis, Methodology, Software, Visualization, Writing – original draft, Writing – review & editing. **Derong Luo:** Funding acquisition, Investigation, Project administration, Resources, Supervision, Validation, Visualization, Writing – review & editing. **Zhongqi Li:** Supervision, Validation, Visualization. **Fei Yu:** Supervision, Validation, Visualization, Writing – original draft, Writing – review & editing.

Declaration of competing interest

The authors declare that they have no known competing financial interests or personal relationships that could have appeared to influence the work reported in this paper.

References

[1] Q.X. Yang, P.C.H. Zhang, L.H. Zhu, et al., Key fundamental problems and technical bottlenecks of the wireless power transmission technology, Trans. China Electrotech. Soc. 30 (5) (2015) 1–8, https://doi.org/10.3969/j.issn.1000-6753.2015.05.001.
[2] J.L. Jia, X.Q. Yan, Research tends of magnetic coupling resonant wireless power transfer characteristics, Trans. China Electrotech. Soc. 35 (20) (2020) 4217–4231, https://doi.org/10.19595/j.cnki.1000-6753.tces.191102.
[3] K. Aditya, V.K. Sood, S.S. Williamson, Magnetic characterization of unsymmetrical coil pairs using archimedean spirals for wider misalignment tolerance in IPT systems, IEEE Transactions on Transportation Electrification 3 (2) (2017) 454–463, https://doi.org/10.1109/TTE.2017.2673847.
[4] M. Budhia, J.T. Boys, G.A. Covic, et al., Development of a single-sided flux magnetic coupler for electric vehicle IPT charging systems, IEEE Trans. Power Electron. 60 (1) (2013) 318–328, https://doi.org/10.1109/iecon.2010.5675408.
[5] A. Zaheer, G.A. Covic, D. Kacprzak, A bipolar pad in a 10-kHz 300-W distributed IPT system for AGV applications, IEEE Transactions on Industrial Electronics 61 (7) (2014) 3288–3301, https://doi.org/10.1109/TIE.2013.2281167.
[6] S. Kim, G.A. Covic, J.T. Boys, Tripolar pad for inductive power transfer systems for EV charging, IEEE Trans. Power Electron. 32 (7) (2017) 5045–5057, 10.1109/TPEL. 2016. 2606893.
[7] A. Ahmad, M.S. Alam, A.A.S. Mohamed, Design and interoperability analysis of quadruple pad structure for electric vehicle wireless charging application, IEEE Transactions on Transportation Electrification 5 (4) (2019) 934–945, https://doi.org/10.1109/TTE.2019.2929443.
[8] S.Y. Jeong, S.Y. Choi, M.R. Sonapreetha, et al., DQ-quadrature power supply coil sets with large tolerances for wireless stationary EV chargers, in: 2015 IEEE PELS Workshop on Emerging Technologies: Wireless Power (2015 WoW), IEEE, Daejeon, 2015, pp. 1–6, https://doi.org/10.1109/WoW.2015.7132800.
[9] Zh Zhang, K.T. Chau, Homogeneous wireless power transfer for move-and-charge, IEEE Trans. Power Electron. 30 (11) (2015) 6213–6220, https://doi.org/10.1109/TPEL.2015.2414453.
[10] S.Y.R. Hui, W.W.C. Ho, A new generation of universal contactless battery charging platform for portable consumer electronic equipment, IEEE Trans. Power Electron. 20 (3) (2005) 620–627, https://doi.org/10.1109/TPEL.2005.846550.
[11] W.X. Zhong, X. Liu, S.Y.R. Hui, A novel single-layer winding array and Receiver coil structure for contactless battery charging systems with free-positioning and localized charging features, IEEE Trans. Power Electron. 58 (9) (2011) 4136–4144, https://doi.org/10.1109/TIE.2010.2098379.
[12] M. Budhia, G. Covic, J. Boys, A new IPT magnetic coupler for electric vehicle charging systems, in: IECON 2010-36th Annual Conference on IEEE Industrial Electronics Society, IEEE, Glendale, AZ, USA, 2010, pp. 2487–2492, https://doi.org/10.1109/IECON.2010.5675350.
[13] G. Yang, D. Shuai, Ch Zhu, et al., Design of a high lateral misalignment tolerance magnetic coupler for wireless power transfer systems, in: 2017 IEEE PELS Workshop on Emerging Technologies: Wireless Power Transfer (WoW), IEEE, Chongqing, China, 2017, pp. 34–39, https://doi.org/10.1109/WoW.2017.7959361.
[14] Y. Chen, R. Mai, Y.Y. Zhang, et al., Improving misalignment tolerance for IPT system using a third-coil, IEEE Trans. Power Electron. 34 (4) (2019) 3009–3013, https://doi.org/10.1109/TPEL.2018.2867919.
[15] P.C. Zhang, M. Saeedifard, O.C. Onar, et al., A field enhancement integration design featuring misalignment tolerance for wireless EV charging using LCL topology, IEEE Trans. Power Electron. 36 (4) (2021) 3852–3867, https://doi.org/10.1109/TPEL.2020.3021591.
[16] Z.Q. Li, X.B. Xiong, L.Q. Ren, et al., Design and optimization of Quasi-Constant coupling coefficients for superimposed dislocation coil structures for dynamic wireless charging of electric vehicles, Progress In Electromagnetics Research M 116 (2023) 23–38, https://doi.org/10.2528/PIERM22120802.
[17] S. Choi, S. Tetong, Ultraslim S-type power supply rails for roadway-powered electric vehicles, IEEE Trans. Power Electron. 30 (11) (2015) 6456–6468, https://doi.org/10.1109/TPEL.2015.2444894.
[18] Z. Li, J. Yi, Modeling and design of a transmission coil and four cascaded receiving coils wireless charging structure with lateral misalignments, IEEE Access 8 (2020) 75976–75985, https://doi.org/10.1109/ACCESS.2020.2988888.
[19] Z. Wang, C. Hu, Design of magnetic coupler for inductive power transfer system based on output power and efficiency, Transactions of China Electrotechnical Society 30 (19) (2015) 26–31.